

THE SPECTRAL EVOLUTION OF GALAXIES. I. AN OBSERVATIONAL APPROACH¹DONALD HAMILTON²

Department of Physics and The Enrico Fermi Institute, University of Chicago; and Kitt Peak National Observatory

Received 1985 February 22; accepted 1985 April 23

ABSTRACT

We have conducted a major new spectrophotometric survey of giant elliptical galaxies in order to measure changes due to spectral evolution. The data set consists of good spectrophotometry on 33 galaxies to a redshift of $z = 0.8$. The look-back time for this redshift, $H_0 \approx 50 \text{ km s}^{-1} \text{ Mpc}^{-1}$, $q_0 \approx 0$, is 7–8 Gyr, which is about half the age of the universe.

Our objects were chosen from a new multicolor (*ugri*), multifield survey using the prime focus cameras of the KPNO and CTIO 4 m telescopes. All plates were scanned by a microdensitometer and reduced with the KPNO implementation of FOCAS. Our primary selection criterion was redness in color-color diagrams. The galaxies selected for the spectrophotometric program were not always the reddest giant elliptical galaxies, but an attempt was made to sample along the perceived color distribution of these galaxies. It is hoped that this procedure reduces any potential biases. This is the first survey to be conducted which selects program objects according to optical colors. We intentionally did not select galaxies which are members of the cores of rich clusters of galaxies; those observed are also known not be radio sources. No other survey has yet been conducted in this manner or spirit, with control over known selection effects.

The amplitude of the 4000 Å break was used as the indicator of spectral evolution. The data of the evolution diagram (redshift vs. break amplitude) indicate that a change of less than 7% in the break amplitude is evident at the high-redshift end, $z \approx 0.8$. These data also indicate that giant elliptical galaxies are much older than 8 Gyr, and within simple Friedmann models we suggest, therefore, H_0 is less than $70 \text{ km s}^{-1} \text{ Mpc}^{-1}$ for $q_0 \approx 0$. Only for $H_0 \lesssim 32 \text{ km s}^{-1} \text{ Mpc}^{-1}$ is $q_0 > 0.5$ possible.

The observed width of the break amplitude distribution for all program galaxies indicates the validity of the assumption of coevality to within ± 2 Gyr to a redshift of $z \approx 0.8$.

Extension of the evolution diagram to higher redshifts ($0.8 < z < 1.0$) will provide valuable constraints on galaxy evolution and help enlighten our knowledge of any potential biases that the red-selection criteria may have introduced.

Subject headings: cosmology — galaxies: evolution — galaxies: photometry — spectrophotometry

I. MOTIVATION

It was realized very early on in the establishment of the cosmological problem that at sufficiently high redshifts (or large light-travel times) the character of the light from distant galaxies would be different from that of low-redshift objects of the same type (Hubble and Tolman 1935). The difference would arise from having different main-sequence turnoff points; the more distant galaxies would have a younger population of stars. The character of the light in the ultraviolet-blue region of the spectrum would, therefore, become systematically bluer with increasing redshift. This is illustrated in Figure 1, where the hydrogen-burning lifetime of some main-sequence stars is displayed along with the redshift and look-back time for various values of the deceleration parameter q_0 . It is through this relation that the hydrogen-burning lifetime of stars determines the evolutionary rate of change to the intrinsic light of galaxies. The time scale for cosmology is set through the Hubble constant.

The gradient of this bluing effect with redshift is also depen-

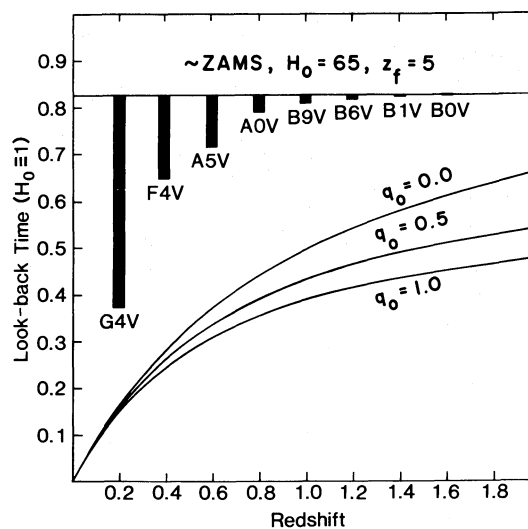


FIG. 1.—Look-back time as a function of redshift. In order to place the look-back time on an absolute basis we have assumed that $H_0 = 65 \text{ km s}^{-1} \text{ Mpc}^{-1}$. Length of black bar schematically represents lifetime of a star. Redshift of formation is $z = 5$, corresponding to a look-back time of 12.8 Gyr for $H_0 = 65 \text{ km s}^{-1} \text{ Mpc}^{-1}$ and $q_0 = 0$. We have assumed spectral types for an approximate zero-age main sequence. Stellar ages from Iben (1967).

¹ Presented as a thesis to the Department of Physics, University of Chicago, in partial fulfillment of the requirements for the Ph.D. degree.

² Visiting Scientist, Kitt Peak National Observatory and Cerro Tololo Inter-American Observatory, National Optical Astronomy Observatories, which are operated by AURA, Inc., under contract to the National Science Foundation.

dent on how many stars evolve at what rate off the main sequence (or the slope of the initial mass function, Tinsley 1967, 1972*a, b, c*, 1980; Tinsley and Gunn 1976), on the star formation history of the galaxy, and on the formation time of galaxies. Because of the great variety of galaxy morphologies available, we shall restrict our discussion of the spectral evolution of galaxies to the simplest class, i.e., that of a single-burst production of stars. (We define a single-burst population of stars to be those generations of stars produced in a single instigation of star formation.) These populations of stars will be presumed to be a close approximation to elliptical galaxies and, in particular, giant elliptical galaxies. The latter group seems to have been particularly efficient in converting gas into stars during the initial collapse of the protogalaxy. Evolutionary models of these galaxies (Tinsley 1972*a, c*; Bruzual 1983; this paper) indicate that this assumption is a reasonable one.

For any problem concerning the redshift-magnitude diagram (Hubble diagram) and corrections thereto, what is ultimately desired is the change in absolute luminosity as a function of time or redshift. In order to study the concomitant problem, the star formation history of these galaxies, a more appropriate indicator is some color index, e.g., x/y , where in the simplest formulation x is some measurement of the ultraviolet flux density (young star component) and y is a measurement of the far-red to infrared flux density (or evolved star component which can also include young stars). In order to obtain the time derivative of the intrinsic luminosity, we need to resort to models of galaxy evolution. The evolutionary modeling technique is a first approximation, and the more detailed formulations of Renzini (1981) and of Renzini and Buzzoni (1983) are the logical next step.

This paper discusses two major new surveys, one photometric and the other spectrophotometric. A more specific discussion of the problem and detection of the spectral evolution of galaxies is presented in § II. The new photometric survey is discussed in § III. Properties of our "evolution indicator," the 4000 Å break amplitude, are presented in § IV. Section V is a description of the spectrophotometric survey. Section VI is a discussion of our version of galaxy evolution models styled after those of Bruzual and Tinsley. Finally, § VII is a discussion of the results and the implications for observational cosmology. For those readers uninterested in details, we recommend proceeding directly to this section.

II. INTRODUCTION

There are several potential methods by which the spectral and luminosity evolution of galaxies could be measured. A widely used technique, that of the number-magnitude relation for galaxies, is believed to be an indicator of the history of spectral and luminosity evolution (Brown and Tinsley; Tinsley 1977). An alternative method is spectrophotometric and will involve a much less sizable sample than that available from areal surveys. This latter technique is much more time-consuming but will yield more readily interpretable results, assuming that selection effects are properly controlled.

a) Spectrophotometry and The Evolution of Galaxies

A more straightforward approach to the measurement of any signature of spectral evolution is spectrophotometry of individual sources. This technique obviates the need for K -corrections altogether. Also, if care is taken the information content is far greater in low signal-to-noise ratio spectro-

photometry than that obtainable with high signal-to-noise ratio broad-band photometry.

Several attempts in the past have been made to detect evolutionary effects. Oke (1971) compared spectrophotometry of several galaxies with redshifts ranging from $z \approx 0.2$ to $z \approx 0.5$. He found no discernable difference between the spectral energy distributions of his three program galaxies.

The first major effort to detect evolution was by Wilkinson and Oke (1978) using the spectrophotometry of Gunn and Oke (1975). They concluded that the dispersion among the spectral energy distributions of their program galaxies was too large to justify any conclusions about evolutionary effects. They believed that the dispersion was due to variations in the amount of reddening and to metallicity differences. In their comparisons they analyzed over a large wavelength range, and certainly their results would be affected by the same problems that afflict broad-band studies.

Spinrad (1977, 1980) and Spinrad's data published in Bruzual (1983) have demonstrated the possible existence of evolutionary effects. Most spectrophotometric surveys of high-redshift galaxies (and infrared studies based on these data) have primarily concerned 3CR sources. It is generally assumed, but never proven, that these program objects constitute a homogeneous population. Optical imaging surveys of the more distant objects (Djorgovski, Spinrad, and Marr 1984) indicate that this assumption is probably an incorrect one. In addition, the width and shape of the distributions of intrinsic optical luminosities and of the colors for the low-redshift 3CR galaxy sample are different (broader and bluer) from that of nonradio first-ranked cluster galaxies (Sandage 1972*b*), which makes these objects less than ideal standard candles. Also, van den Bergh (1975) has noted that the radio activity is correlated with bursts of star formation and with the presence of emission lines. The probability of obtaining a redshift is usually proportional to the emission line strength to continuum ratio.

Finally, we should note that no spectra have been published of most of these 3CR sources. It is very difficult to assess the homogeneity of this sample without such data.

b) This Spectrophotometric Survey for Galaxy Evolution

We take an alternative approach in our selection of objects. Instead of selecting on the basis of radio power, or on first-ranked cluster status, or even just on apparent magnitude, we impose a criterion in order to select a more homogeneous sample of objects with good control on the selection. This criterion is redness in the optical bandpasses of the *ugri* photometric system (Hamilton 1985).

The advantages of selecting the reddest galaxies are that (1) it reduces the possibility of residual or episodic star formation which is difficult to model, hence we would tend to select those galaxies which are a single, almost coeval population of stars; (2) given the correlation between color and magnitude (Baum 1959; Sandage 1972*a*; Faber 1973, 1977), the reddest galaxies are the intrinsically brightest; (3) these objects are easily found on multicolor areal surveys; (4) most modern detector systems are red-sensitive; and (5) since redness and the break amplitude are positively correlated, maximizing redness increases the contrast, hence detectability, of the break.

Since no survey met our stringent criteria (deep, long-wavelength coverage, and multifield), we instigated one ourselves. A description of this survey is given in the next section. This survey provided us with sufficient leverage to control more effectively selection effects.

Once the multicolor selection criteria had been established, it was necessary to design a suitable spectrophotometric program. A good indicator of stellar evolution is something that resembles the color index ($U-I$). However, given that most spectrophotometers do not cover a range of 7000 Å, a more tractable coverage would be ($U-B$), in the rest frame. Spinrad (1977, 1980) has demonstrated the utility of this approach. An observable equivalent to that of ($U-B$) is the amplitude of the 4000 Å break, and unlike most color indices it is essentially monochromatic. The 4000 Å break amplitude is defined as the ratio of the average of flux densities above and below 4000 Å. Designing a program around this line feature is convenient, in that it is also used as a redshift indicator.

It turned out that our redness selection criterion was sufficient to select a large number of non-rich-cluster galaxies, and so the effects of dynamical evolution, if at all present, are reduced. A problem might exist, however, in that at our faintest levels ($r \approx 23$ mag) there is not sufficient depth remaining beyond this level to detect fainter cluster members if they exist. Only higher signal-to-noise ratio imaging will resolve this question.

III. THE SURVEY

In an ideal situation, a properly selected sample would be homogeneous in the type of galaxy observed and selected so as to be uniformly distributed in redshift. These two constraints imply a selection based on redshift and color. Unfortunately, the two observables are not completely independent.

Surveys for galaxies have usually relied on the relation of apparent magnitude to redshift. By surveying in only one bandpass, such as V , the hypothesis is usually made that the apparent magnitude and redshift are uniquely correlated. This is, of course, not quite true. This assumption is valid only when the distribution of galaxies is of a single type with a specific luminosity. Because of K -corrections, galaxies which are one color at z_1 may not be considered red (or blue) at another redshift z_2 where $z_2 > z_1$. This problem of selection can be somewhat obviated by first deciding on the galaxy type to be surveyed, e.g., giant elliptical galaxies, and then applying the constraints imposed by this to the observational program.

In order to have a sufficient number of program objects to choose from, a large areal survey was necessary. A technical requirement for the spectrophotometric survey was that we could only select an object that was within 3' of a sufficiently bright offset star. This helped ensure accurate offsetting of the Mayall telescope.

We also desired to search for galaxies to reasonably faint limits ($r \approx 23$ mag) in order to obtain a sample of objects at very high redshifts ($0.5 < z < 1.0$). Another requirement was that at the fainter levels we needed good image scale so as to sample the image profile in the digitization process well.

All these requirements necessitated a new survey to be conducted in several bandpasses or colors. The best instrument for this purpose was the prime-focus triplet corrector cameras of the KPNO and CTIO 4 m telescopes. Details of the survey are given in Hamilton (1983), but for completeness we will give a brief description of our procedures. Details of the $ugri$ photometric system, its calibration and renormalization, will be presented in the next paper in this series (Hamilton 1985). The multifield quasar counts of Hamilton (1983) relied on instrumental magnitudes $u'jfn$ and not the fully calibrated $ugri$.

Photographic plates using Kodak fine-grained emulsions IIIa-J, IIIa-F, and IV-N were exposed through filters UG5,

GG385 for the IIIa-J emulsion, GG495 for IIIa-F, and RG695 for IV-N. Typical exposure times were 180 minute for the ultraviolet, 45–90 minute for the blue and red plates, and 45 minutes for the far-red emulsion. The far-red plates were hypersensitized using the $AgNO_3$ process of Schoening (1978).

The area of the exposed prime focus image is about 0.8 deg². Of this total area we digitized an area of 0.5 deg². We used the KPNO PDS microdensitometer in a raster scan mode digitizing a 6600 × 6600 pixel image using a 20 μm (0'37) aperture. Each of these digital images was reduced using the KPNO version of FOCAS (Valdes 1983a, b). A detection was considered real if it was at least five contiguous pixels and at least 2.5 standard deviations above local sky, after some mild smoothing. A catalog for each plate of about 20,000 objects was produced. This scanning/reduction procedure was performed on each of the four bandpasses of a particular field. After the boundaries of the two-dimensional image classification scheme were determined and applied (Valdes 1983b), the four catalogs were matched. This survey yielded about 300,000 objects to $g \approx 24$ mag with each object in four colors ($ugri$).

Some properties of the fields surveyed are given in Table 1. These fields were specifically chosen because of their low reddening values, as given by Burstein and Heiles (1982). For all the fields, with the possible exception of SA 68, the color excesses are negligible to within the errors (of at least ~ 0.06 in E_{B-V}), and therefore we made no attempt at correcting the colors or the subsequent spectrophotometry for reddening due to our Galaxy.

The galaxies chosen in each magnitude interval were selected relative to the color distribution of all galaxies in that same magnitude range. The diagrams chosen for the selection were either ($u-g$) versus ($g-r$) or ($g-r$) versus ($r-i$) for the brightest objects selected ($18 < r < 19$), ($g-r$) versus ($r-i$) for the intermediate r -magnitudes ($19 < r < 21$), and ($r-i$) only for the faintest sample ($22 < r < 24$). This approach is designed to choose the same type of galaxy at all redshifts.

Each potential program object was examined on the r - and i -plate material to ensure that it was actually a galaxy. At the fainter levels, where the colors of high-redshift galaxies become very red and noisy and where the image structure is dominated principally by atmospheric turbulence, it was felt that the probability of mistaking an M dwarf for a galaxy was too high a risk. Also, the red triplet corrector (BK-7) of the Mayall telescope has zonal irregularities which negate the classification process in practice. Although the efficiency of the resolution classifier is quite good at the fainter levels (Hamilton 1983), we consider a well-trained eye to be the ultimate discriminator.

TABLE 1
PRIME FOCUS/FOCAS SURVEY FIELDS

Field	l	b	$E(B-V)$
SA 68.....	112°	-46°	0.03
SGP.....	290	-89	0.00
ST.....	191	-62	0.00
RW.....	238	-43	0.00
AB.....	216	-35	0.02
Lynx.....	177	+37	0.02
SA 57.....	69	+86	0.00
Hercules.....	77	+35	0.02

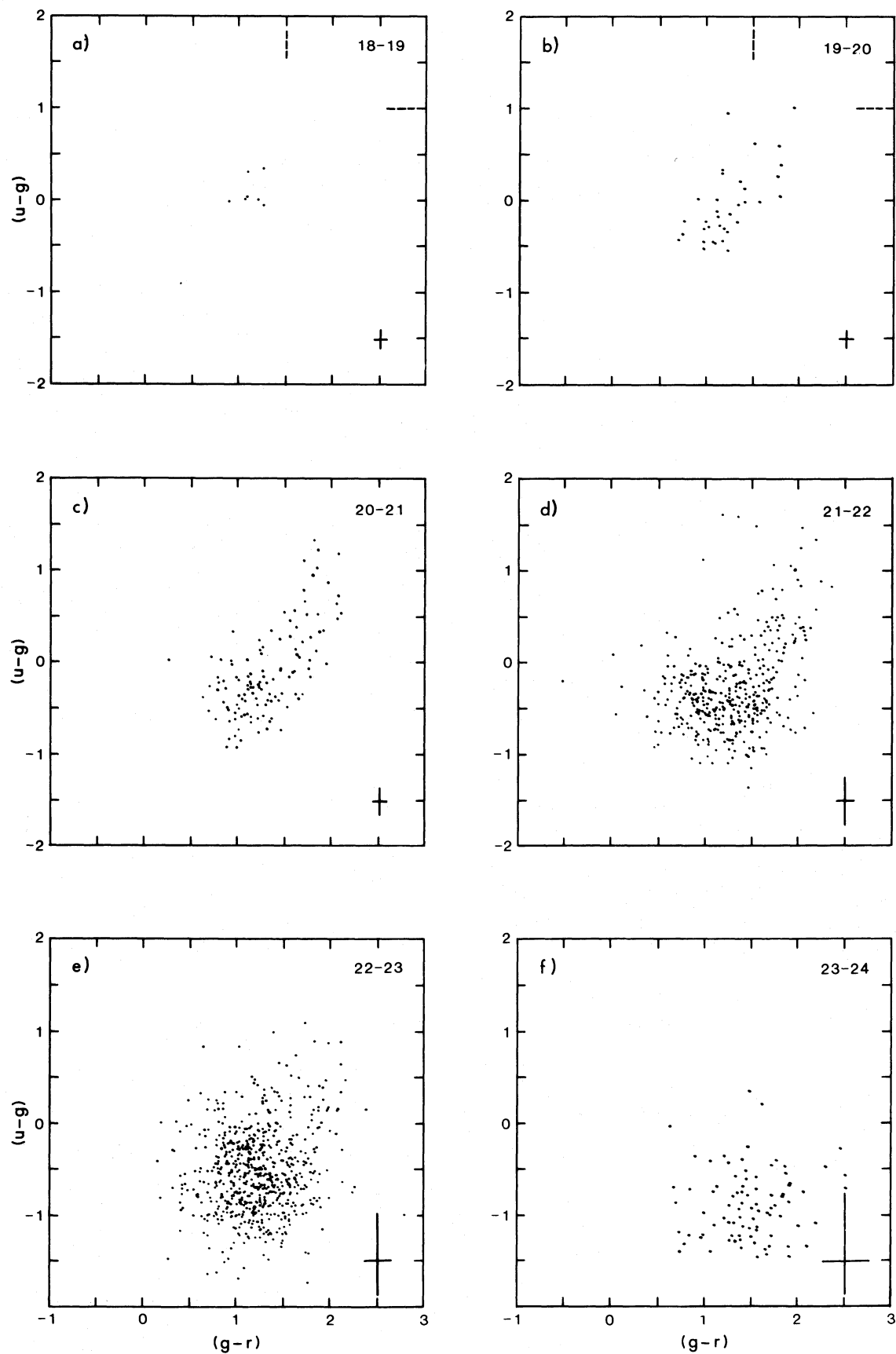
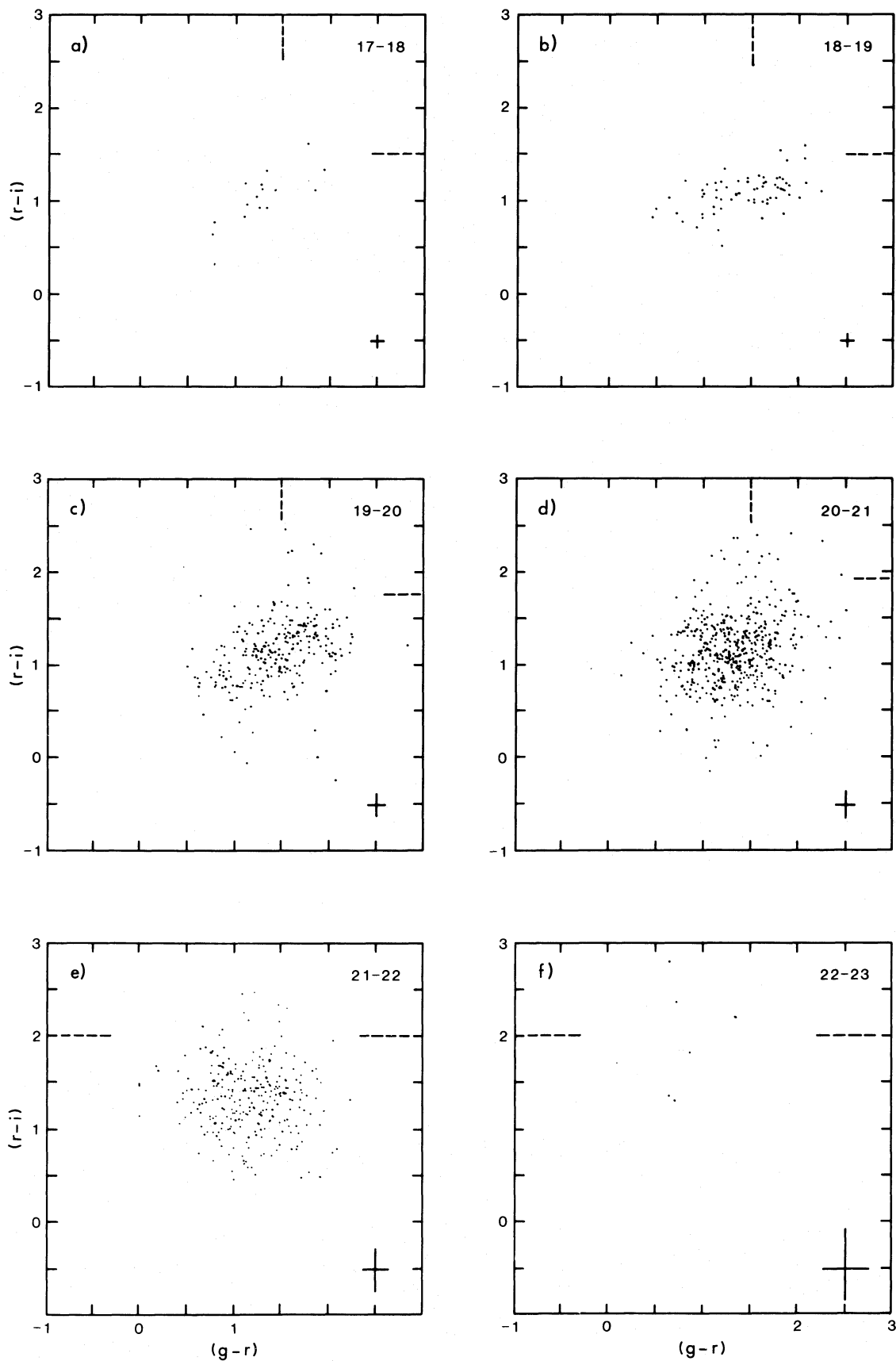


FIG. 2.—Diagrams of galaxy $(u - g)$ vs. $(g - r)$ for one of the prime-focus/FOCAS survey fields, Hercules 1. Numbers in upper right corner define the g -magnitude interval for that diagram. Partial dashed lines are the boundaries of the area from which we selected red galaxies for the spectrophotometric program. Error bar indicates photometric precision obtained, within that magnitude interval and for an object with a typical color index.

FIG. 3.—Same as Fig. 2, for $(g-r)$ vs. $(r-i)$

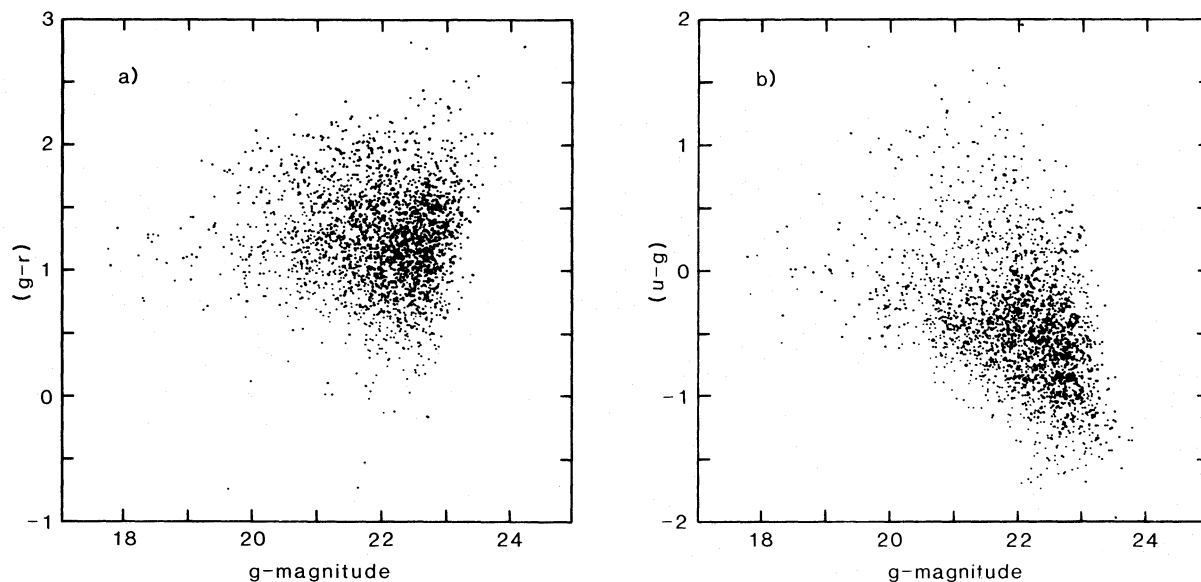


FIG. 4.—Color-magnitude diagrams of (a) $(g-r)$ vs. g -magnitude and (b) $(u-g)$ vs. g -magnitude of galaxies for the survey field Hercules 1.

In Figures 2 and 3 we present $(u-g, g-r)$ and $(g-r, r-i)$ two-color diagrams of galaxies for one of our survey fields. In Figures 4 and 5 we present color-magnitude diagrams. The boundaries of the regions where a candidate galaxy must reside in the color-color diagrams are indicated by the partial dashed lines on Figures 2 and 3. Figures 2–5 are for the data of the Hercules 1 field. Since not all the fields are fully calibrated yet, it is not possible to present absolute colors for all the program objects. If an object did reside in the red zone portion of Figures 2 and 3, it was then examined on all the relevant plates by eye to ensure that it was near a bright enough offset star, it was really resolved, and the colors were approximately correct. Spurious colors can result if there are emulsion scratches or noise sufficiently near the object.

It has been known for several years that as the sampling depth is increased the $(g-r)$ color-index of galaxies becomes

increasingly bluer (Kron 1978). This behavior has almost universally been believed to be a result of galaxy evolution. For the $(u-g)$ and $(g-r)$ colors we confirm the bluing trend as noted by Kron (1978). However, quite unexpectedly there appears to be a trend towards redder colors in the diagrams with $(r-i)$, as illustrated in Figure 3.

The observed color-color distribution is not a single distribution but is a superposition of several distributions, each characterized by a particular type of galaxy. Our selection by color does not choose the reddest galaxy in the red zone, but is more an attempt to sample representatively what we perceive to be the color distribution of giant elliptical galaxies. We estimate that the dispersion in rest-frame colors is approximately 0.5 mag. This number is difficult to accurately estimate at this time since the survey is, as yet, not fully calibrated, and the objects observed are in several different fields.

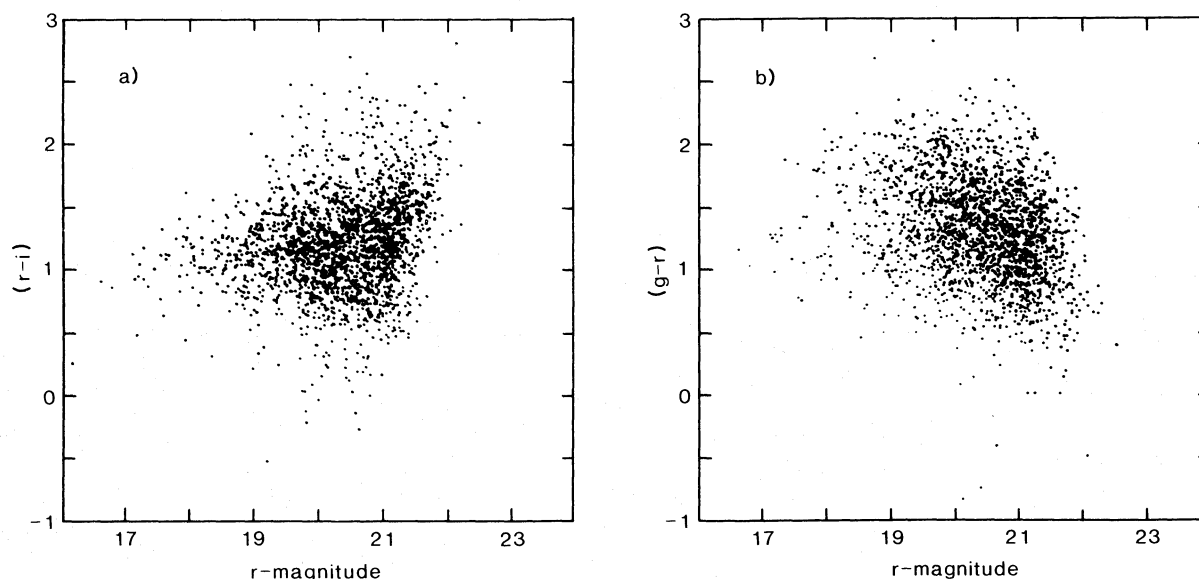


FIG. 5.—Color-magnitude diagrams of (a) $(r-i)$ vs. r -magnitude and (b) $(g-r)$ vs. r -magnitude of galaxies for the survey field Hercules 1.

IV. THE PROPERTIES OF THE 4000 Å BREAK

a) Introduction to and Definition of the 4000 Å Break

In this section we present some qualitative information on the behavior of the amplitude of the 4000 Å break with respect to known stellar and galaxy properties. We have used several published stellar and galaxy spectrophotometric catalogs for this analysis. The two stellar catalogs are Gunn and Stryker (1982) and Jacoby, Hunter, and Christian (1984). The galaxy sample was obtained from Heckman, Balick, and Crane (1980).

Before we begin this discussion of correlations it is necessary to define exactly what we mean by the amplitude of the 4000 Å break. The break is defined as the ratio of the average flux density between 4050 and 4250 Å to that between 3750 and 3950 Å, where flux density is in units of $\text{ergs s}^{-1} \text{cm}^{-2} \text{Hz}^{-1}$. We decided after some analysis to use the definition of Spinrad (Bruzual 1983), not only for consistency but also because this definition (here using f_v or the related f_λ definition) is relatively insensitive to noise (see § IVe).

The break is due to the sudden onset of stellar photospheric opacity shortward of 4000 Å (Öhman 1934). This sudden onset is due not just to the Fraunhofer H and K lines of Ca II but to a variety of elements heavier than helium in various stages of ionization. It is expected that the 4000 Å break will correlate with effective temperature, surface gravity, and metallicity. It is our aim to use the break measurement as a temperature indicator for the integrated stellar population.

b) Stellar Properties of the 4000 Å Break

The first important investigations of the properties of the 4000 Å break were by van den Bergh (1963) and by van den Bergh and Sackmann (1965). They demonstrated that Δ (their measurement of the break) depends on stellar metallicity. Because of the definition of the 4000 Å break, it is expected that it will correlate well with other stellar metallicity indicators such as Q39 of Zinn (1980), $\delta_{(U-B)}$, and m_1 of Strömgen (1966).

The variation of the 4000 Å break with stellar spectral type (or effective temperature) is depicted in Figure 6. The data were obtained from the spectrophotometry of Gunn and Stryker (1982), as were the spectral classifications. Given that errors in spectral classification exist, the segregation of the giant stars from those of the main sequence is remarkably good for the spectral types later than $\sim G0$. Some of the scatter in Figure 6 is probably due to misclassifications and to metallicity variations. The scatter at the red end is enhanced due to the lower signal-to-noise ratio of those data.

A photospheric line which is expected to contribute significantly to the 4000 Å break is the K line of Ca II at 3933 Å. This line is more sensitive to metallicity than to the stellar population. The correlation between the 4000 Å break and the Ca II K line index is presented in Figure 7a, and it indicates that giant stars contribute nearly all the Ca II K line absorption for spectral types later than $\sim G0$.

A stellar line feature which should correlate well with the break is the group of Mg atomic lines ("Mg b") between 5167 and 5184 Å and the MgH molecular bandhead at 5211 Å. It is well known that a line index measuring this region correlates well with temperature, surface gravity, and metallicity (Fitch and Morgan 1951; Faber *et al.* 1985; O'Connell 1973; Spinrad 1961; Mould 1978). Figure 7b demonstrates the good correlations between a line index measurement of Mg b + MgH and the break amplitude. The effect of surface gravity is quite apparent.

The G band (due to CH and atomic lines with the bandhead at 4314 Å) is expected to have mild direct influence on the 4000 Å break amplitude, as the majority of the absorption occurs at wavelengths longward of the upper interval of the 4000 Å break definition. Since the G band is known to be a strong temperature indicator (O'Connell 1973; Spinrad and Taylor 1971), a correlation would therefore exist, as Figure 7c confirms. The G band is insensitive to metallicity and to surface gravity. There is no luminosity segregation apparent from Figure 7c.

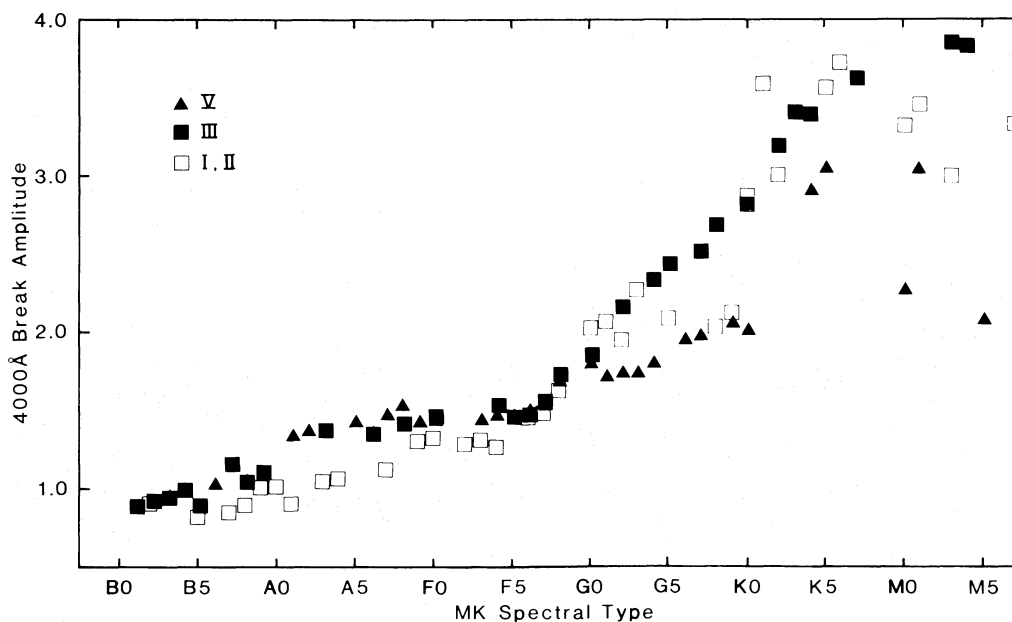


FIG. 6.—Variation of amplitude of 4000 Å break with respect to Morgan-Keenan spectral types. Values of break calculated from the Gunn-Stryker spectrophotometric atlas; spectral types from Gunn and Stryker (1982). Luminosity classes indicated by filled triangles, dwarfs; filled squares, giants; squares, supergiants.

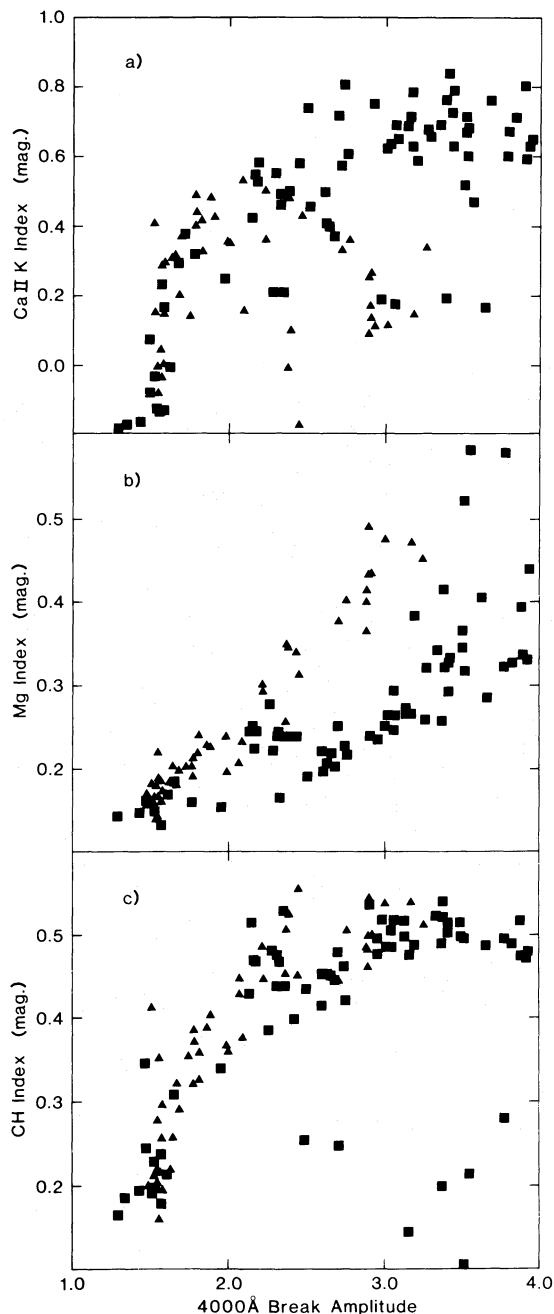


FIG. 7.—4000 Å break amplitude vs. stellar line index features: (a) Ca II K line index, (b) Mg index, (c) CH (G-band) index. Line indices from Gunn and Stryker (1982). Luminosity classes indicated as in Fig. 6.

c) Galaxy Properties of the 4000 Å Break

We have analyzed a subset of the image-dissector scanner data of Heckman, Balick, and Crane (1980) which was kindly made available to us by Dr. T. Heckman. We measured the 4000 Å break amplitude for ~ 70 of the galaxies in this sample (hereafter, the large sample). Another subset was selected on the basis of the late-type (Morgan sense) appearance of the spectrum (hereafter, the small sample). The measurements of the 4000 Å break were compared with measurements of the line features at H δ , 3933 Å, and 4314 Å. The Heckman, Balick, and Crane data were all obtained with a 6" aperture and pri-

marily represent nuclear values. Observing a set of galaxies distributed in size and redshift with a fixed aperture results in a larger dispersion in relative properties than would have been observed if a metric aperture had been used. We also examined the data for correlations with absolute magnitude and with published ($U-B$) and ($B-V$) nuclear colors of these galaxies. The UBV photometry was taken from the compilation of Longo and de Vaucouleurs (1983) and comes from a variety of sources.

In the ultraviolet, the predominant stellar contributors to the flux density will be stars earlier than about F5, if such stars exist. These stars will also increase the equivalent width of the Balmer series. Figure 8a demonstrates the good anticorrelation between the H δ equivalent width and the break amplitude. To the extent that the equivalent width of H δ could be considered to be an age indicator, so could the 4000 Å break, i.e., they measure essentially the same phenomenon. H δ was chosen as

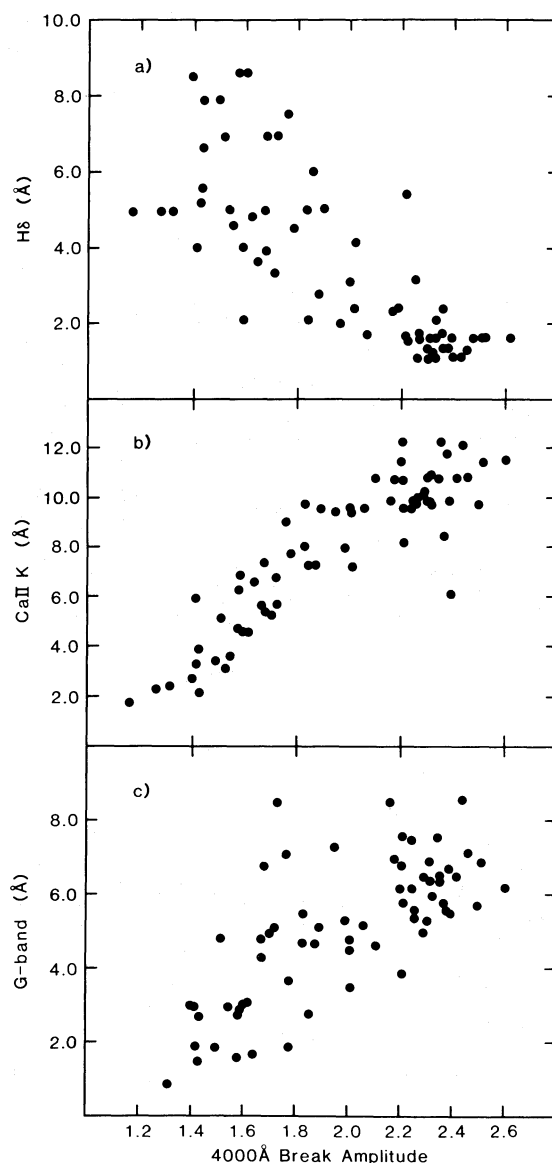


FIG. 8.—Correlations between 4000 Å break amplitude and several line indices (measured as equivalent widths) for 71 galaxies of Heckman, Balick, and Crane (1980): (a) H δ equivalent width, (b) Ca II K equivalent width, (c) G-band equivalent width.

the Balmer line to measure in these galaxies, as $H\beta$ is often contaminated with emission.

In Figures 8b and 8c it is apparent that the equivalent widths of the Ca II K line and the G band (4314 Å) for the large galaxy sample correlate very well with the break amplitude, thus indicating equivalent information content.

Malmquist bias might enter in the selection of objects for the spectrophotometric program if the amplitude of the break is positively correlated with intrinsic luminosity. (Malmquist bias is the difference between the results of observations based on a distance-limited sample and those based on an apparent magnitude-limited sample.) Such an effect would not be expected to be significant except for the objects of lowest luminosity. To check for such a correlation we have examined the relations between absolute magnitude and break amplitude, an Mg + MgH index, and a Ca II K line index for the large galaxy sample. These are all shown in Figure 9. In none of these is a correlation evident. Even Faber (1977) has noted that the Mg_2 versus M correlation for local galaxies is a poor one. The large dispersion in both Faber's diagram and in Figure 9 may be due to local supercluster effects. More impor-

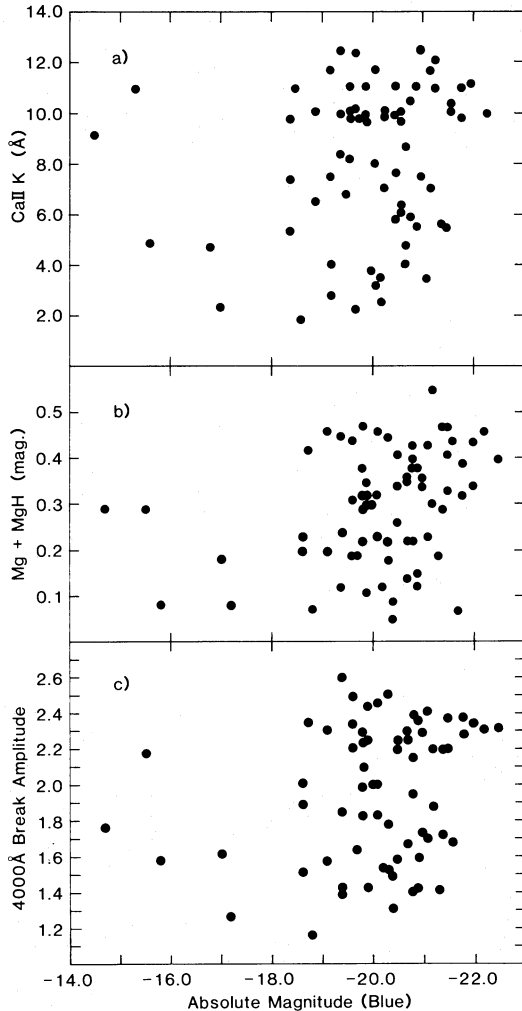


FIG. 9.—Scatter diagrams of several line indices with absolute blue magnitude: (a) Ca II K line index, (b) Mg b + MgH, (c) 4000 Å break amplitude. Break amplitudes calculated from spectra of Heckman, Balick, and Crane (1980), absolute magnitudes from that paper.

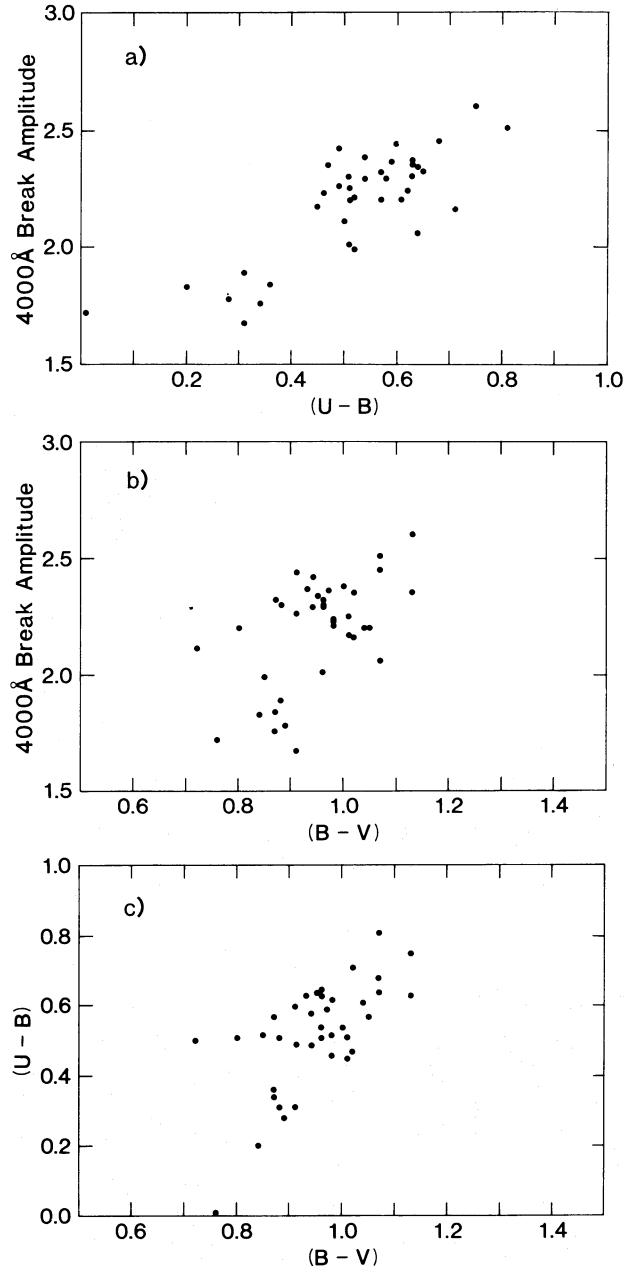


FIG. 10.—(a) Correlation between 4000 Å break amplitude and color index ($U - B$). (b) Correlation between 4000 Å break amplitude and color index ($B - V$). (c) ($U - B$) vs. ($B - V$) diagram for the same data as in (a) and (b).

tantly, the color-magnitude distributions for the galaxies in Coma and Virgo as obtained by Visvanathan and Sandage (1977) tend to level off at the red end, and so for red-selected galaxies little correlation would be expected. The result of the Malmquist bias would be to redden the distribution at the faint or high-redshift end. The absolute magnitudes were taken from Heckman, Balick, and Crane (1980).

For the small galaxy sample, we also examined for correlations between ($U - B$) and ($B - V$) using the smallest aperture UBV data for each galaxy, as listed in Longo and de Vaucouleurs (1983). (The smaller apertures were chosen so as to more closely match the 6" aperture of the spectrophotometric observations.) In Figures 10a and 10b we present the break ampli-

tude versus $(U - B)$ and $(B - V)$ respectively, and in Figure 10c the UBV two-color diagram for the same galaxies. As anticipated, the correlation between break amplitude and $(U - B)$ is fair. The break amplitude versus $(B - V)$ relation is much less well defined. An alternative interpretation is that there exist two distinct spectroscopic groups, and within each group there exists no correlation of the break amplitude with nuclear colors.

A small amount of spectrophotometric data other than that of Heckman, Balick, and Crane (1980) is available from O'Connell (1976, 1980), Whitford (1971), and Wells (1972). All these measurements are from photoelectric single-channel scans. The various measurements of the 4000 Å break amplitude for nearby galaxies are listed in Table 2. All the measurements, when possible, were corrected for reddening by our Galaxy. The dereddening technique is described in § IVd. Typical errors in the measurement of the values of the 4000 Å break amplitude are about 0.07.

The important relation to note from the data of Table 2 is that in general the largest (reddest) values of the break amplitude are for the smallest apertures. Line strength and color gradients are known to exist in late-type galaxies (Faber 1977; Tift 1969).

d) The 4000 Å Break and Internal Reddening

We derived the effect of reddening on the break amplitude primarily to see how sensitive it was to extinction intrinsic to the source. This was accomplished by calculating the break amplitude for various values of E_{B-V} using the parameterization of the Whitford (1958) reddening law by Miller and Matthews (1972). The relation we derived is that for small color-excesses ($E_{B-V} < 1.0$),

$$\frac{d\Delta}{dE_{B-V}} = 0.80 + 0.02E_{B-V},$$

where Δ is the break amplitude.

The effect of extinction due to our Galaxy has been reduced by choosing the survey fields to have low Burstein-Heiles color excesses. If reddening is intrinsic to the source, we have no way to determine it uniquely; however, as just demonstrated, the effect is small.

e) Noise and the Measurement of the 4000 Å Break

In designing the spectrophotometric program, an important consideration was the sensitivity of our "evolution indicator" to noise, i.e., poor signal-to-noise ratio data. An advantage, as mentioned earlier, of the definition we finally adopted was that the derived value was insensitive to noise.

To examine this potential problem more fully we took a high signal-to-noise ratio spectrum (~ 100 per pixel) and degraded it by various amounts of additive Gaussian noise. After a degradation the break amplitude was then calculated. The maximum systematic departure of the break amplitude from its true value was less than 1% even when the degradation was equivalent to a signal-to-noise ratio of < 2 per pixel. Given the sky-limited exposures of the cryogenic camera, it is reasonable to assume that the character of the noise is Poissonian and approximately Gaussian. (Nearly all the exposures were obtained during partial mean.)

This procedure has not taken into account that the redshift cannot be accurately estimated from a low signal-to-noise ratio spectrum. For the objects for which we have obtained spectro-

photometry, the signal-to-noise ratio per pixel is always higher than five, and more typically 10. Redshifts can be very accurately determined from such high quality data. Section Vd is a discussion of measurement errors.

TABLE 2

BREAK AMPLITUDES FOR LOCAL GALAXIES			
NGC	Break	Aperture	Reference
185.....	1.76	6'0	1
205.....	1.57	6.0	1
221.....	2.17	6.0	1
221.....	2.07	15.1	2
221.....	2.17	15.1	3
221.....	2.08	59.5	2
221.....	2.09	119.1	2
224.....	2.51	6.0	1
224.....	2.17	15.1	2
224.....	2.39	31.5	3
2685.....	2.23	6.0	1
2768.....	2.38	6.0	1
2787.....	2.60	6.0	1
2841.....	1.67	6.0	1
2950.....	2.30	6.0	1
2985.....	2.00	6.0	1
3031.....	2.45	6.0	1
3079.....	1.84	6.0	1
3198.....	1.84	6.0	1
3610.....	2.20	6.0	1
3613.....	2.29	6.0	1
3631.....	1.71	6.0	1
3675.....	2.35	6.0	1
3718.....	2.40	6.0	1
3938.....	1.96	6.0	1
3945.....	2.36	6.0	1
3953.....	2.30	6.0	1
3992.....	2.42	6.0	1
3998.....	2.25	6.0	1
4026.....	2.44	6.0	1
4036.....	2.24	6.0	1
4088.....	1.78	6.0	1
4096.....	1.67	6.0	1
4125.....	2.34	6.0	1
4157.....	2.11	6.0	1
4111.....	2.26	6.0	1
4258.....	1.83	6.0	1
4278.....	2.32	6.0	1
4374.....	2.38	10.0	3
4472.....	2.53	10.0	3
4486.....	2.06	6.0	1
4552.....	2.30	10.0	3
4589.....	2.37	6.0	1
4736.....	1.99	6.0	1
4874.....	1.93	59.5	2
5055.....	2.16	6.0	1
5077.....	2.20	6.0	1
5322.....	2.32	6.0	1
5371.....	2.21	6.0	1
5676.....	2.01	6.0	1
5866.....	2.20	6.0	1
5907.....	2.35	6.0	1
5982.....	2.30	6.0	1
6015.....	1.72	6.0	1
6503.....	1.89	6.0	1
6703.....	2.02	59.5	2
7785.....	2.14	59.5	2
gE.....	2.35	39.0	4
gE.....	2.25	115.0	4

REFERENCES.—(1) Heckman, Balick, and Crane 1980. (2) Wells 1972. (3) O'Connell 1976, 1980. (4) Whitford 1971.

V. THE SPECTROPHOTOMETRIC SURVEY

a) Observations

The spectrophotometric observations were carried out using two instruments, both in a spectroscopic long-slit mode. The primary instrument was the cryogenic camera at the Ritchey-Chrétien focus of the Mayall telescope on Kitt Peak. This instrument is a high-efficiency grism spectrograph optically coupled by an $f/1$ Schmidt mirror to a Texas Instruments 800×800 pixel three-phase charge-coupled device. The grisms used were generally $300 \text{ lines mm}^{-1}$ with blazes at either 5910 or 8000 \AA and yielded a spectroscopic resolution of about 15 \AA . This arrangement yielded 4.2 \AA per pixel. Because the sensitivity of the TI CCD decreases rapidly below about 5000 \AA , it was necessary to have a low-redshift cutoff of $z \approx 0.20$ in the sample selection. Integrations ranged from about 800 s for the bright sample ($r \approx 19$) to $16,000 \text{ s}$ for the fainter objects ($r \approx 23$). Exposures beyond about 5000 s were sky-limited. The rms readout noise of the TI chip used is about 8 electrons per pixel. The chip itself is cosmetically very clean and has no bad pixels and only a few partially poor columns on the light-sensitive area. A $2''.5$ or a $3''.17$ wide long slit was used for most of the observations except for those of the run of 1984 October. During this run a $2''.0$ blue offset slit was used to move the spectrum approximately 500 \AA to the blue. The use of the long slit was vital for this project because of the excellent sky subtraction it allows.

The other instrument used was the Ritchey-Chrétien spectrograph with a UV-sensitive 40 mm SIT Vidicon tube on the CTIO 4 m telescope. This instrument was used to obtain data for a set of low-redshift galaxies. A $300 \text{ lines mm}^{-1}$ reflection grating blazed at 4000 \AA was used in first order. A long-slit $2''.0$ wide was used for all the UV SIT Vidicon observations. Exposures ranged from 1000 to 4000 s . Because of the enormous readout noise of this detector (~ 200 electrons per pixel), the exposures were never sky-limited. We were able to obtain tolerable data on only eight galaxies. Problems with the detector's cooling mechanism and with the stability of the grid voltages prevented us from obtaining more data. The spectroscopic resolution was about 20 \AA .

The observations obtained at Kitt Peak were performed during absolute photometric nights. All the data were obtained (at both sites) at low air mass, generally less than 1.5. Correction for atmospheric extinction was done by assuming the standard form and zero point for each site. The observations were generally obtained with the long slit along a great circle through the zenith. In other cases the long slit was rotated so as to bring in another nearby galaxy. These nonprogram galaxies that were observed will be referred to as the *serendipitous* sources.

Besides standard star exposures, additional calibration data obtained were HeNeAr exposures, sky flat-field exposures, and quartz or dome flat-field exposures. Sky flat-field exposures are necessary with the cryogenic camera because of nonuniformities in the illumination of the long slit by the internal quartz lamp. At present there is no intersection between the cryogenic camera data and the UV SIT data due to widely spaced observing runs. Such an exercise is not futile, because the transformation between the break amplitudes for the various instruments may not be one-to-one. Inspection of the common data listed in Table 2 demonstrates the problem.

The two-dimensional spectra obtained from the cryogenic camera and UV SIT were reduced using the software of the

Chicago image processing system developed by the author. The reduction procedures for each of the detectors is sufficiently different to warrant different discussions.

b) Reductions of the Cryogenic Camera Spectra

The spectra obtained from the cryogenic camera were debiased, flat-fielded, and linearized with respect to wavelength in pixel space. (A row is defined as the wavelength dimension; a column is then the spatial dimension.) The linearization was done one row at a time. This is a crude method but it does help remove some of the two-dimensional distortions present in the spectra. Some attempt was made to remove or correct for the variation in the focus level across the CCD chip. Due to lack of time, an efficient algorithm for the restoration has not yet been fully developed. Cosmic rays depositing charge on the chip were not a problem, as the CCD is thin enough not to be very sensitive. The bias level and dark current level for each row was determined from an unexposed region of the CCD chip. Dark current for this CCD chip is virtually negligible.

Once the object had been located on the exposure, sky was subtracted by first isolating rows above and below the object. A third-order polynomial was fitted to each column, and the sky was then interpolated pixel by pixel in the object region. This procedure yielded excellent sky subtraction overall. In the region of intense night-sky lines such as the 5577.35 \AA line of [O I], sky subtraction was fair to good.

The instrumental response function for the cryogenic camera was determined by observing several (~ 4) KPNO IIDS or IRS standard stars per night. The data were supplemented in the red and far-red by the published spectrophotometry of Oke and Gunn (1983) or of Oke (1974) corrected to the system of Hayes and Latham (1975). A single function was determined based on the average of those produced from each standard star. The dispersion in the spectrophotometric zero points at 5500 \AA was determined to be 4%. The error in the relative spectrophotometry is estimated to be about 5%. The cryogenic camera is an excellent spectrophotometer.

c) Reduction of the UV SIT Spectra

The procedures for the reduction of the UV SIT data were different from that of the cryogenic camera. Bias exposures were taken before and after each astronomical exposure. These bias frames were then averaged and subtracted from the astronomical exposure. This was necessary because of the effect that stray magnetic fields have on the interference of electrons scattered from the field mesh with those from the readout beam. This effect produces a sine wave-like amplitude modulation in the dark current which changes with time.

Several dark-current frames were taken with integration times the same as the astronomical exposures. These were taken during the day, and no light leakage was discernable. After the bias level was removed from these dark-current exposures, the frame was smoothed by a three pixel wide running square filter. This smoothing process helped reduce the enormous readout noise of the tube. This smoothed version of the dark-current frame was then subtracted from the astronomical frame. We did not fit to the dark frame a two-dimensional function for subtraction purposes. It was felt that the variation of the dark-current level was of a sufficiently high frequency nature that such a procedure would not have been very representative of the data except for the overall level. Our technique produced remarkably satisfactory results.

Sky subtraction was performed by defining sky regions

adjacent to an object region and linearly interpolating between averages of these sky regions to find the sky value in the object region pixel by pixel. The third-order polynomial interpolation technique did not produce satisfactory results, probably because of the non-Poissonian nature of the SIT noise.

The instrumental response function was determined by observing several spectrophotometric standard stars from the compilation of Stone and Baldwin (1983). The dispersion in zero-point determination is about 10%, and we take this to be representative of the spectrophotometric precision obtainable with this device.

d) Measurement Errors

The predominant source of error in the measurement of the break would be from a poor determination of the redshift. All the spectra are of high signal-to-noise ratio (~ 5 – 10 per pixel), and identification of several line features is possible. The redshifts are all based on at least two features, and more typically three or four. The features most used are Ca II H, K, 4000 Å break, the *G* band, and Mg *b* at 5175 Å. The agreement between the redshifts based on several lines is usually better than 0.005 for any *z*.

There are other sources of error in determining the break: telluric features which are not properly removed, poor flat-fielding, poor sky subtraction, and an incorrect instrumental response function. Checks on the purity of the sky subtraction were made on each sky-subtracted region by examining those areas which should not have been contaminated by any object. There were no residuals to within the errors. If there were non-zero residuals, one or more of several parameters could be adjusted and the process repeated until the results were satisfactory. An additional check was made by adding a fake galaxy with noise to a sky-only frame. The sky-subtracted version agreed with the original for all wavelengths to better than 1%.

Telluric features have not posed a problem yet. We estimate the total error from these sources to be about 5%. Repeated observations indicate that random errors are about 0.10 in the break amplitude (5%).

e) The Data

Table 3 presents the relevant observational data for the program galaxies. In this table we give the field name, the galaxy name for that field, the right ascension and declination, which are good to a few arc seconds for the equinox of 1950.00, the redshift, and the break amplitude. Table 4 presents the same information for the serendipitous galaxies. A spectrum of one of the program objects, Lynx 2: 7116.0, is given in Figure 11. This spectrum was obtained with the cryogenic camera, and its signal-to-noise ratio is typical of that obtained in the spectrophotometric survey.

VI. EVOLUTIONARY MODELS OF GALAXIES

As an aid to understanding how spectral evolution could affect our observations, we developed models based on the evolutionary synthesis technique of Bruzual (1981, 1983) which were fashioned after those of Tinsley (1967, 1972*a*). This technique has the advantage over normal population synthesis (see, e.g., Faber 1972; O'Connell 1976) in that the spectrum of an object can be determined for any time.

The models have two basic ingredients: a star formation rate and an initial mass function. The product of these is proportional to the number of stars of a given mass created in a specified time interval. We have parameterized the star forma-

TABLE 3
SPECTROPHOTOMETRIC SURVEY: PROGRAM GALAXIES

Field	Galaxy	α (1950.00)	δ (1950.00)	<i>z</i>	Break
SA 68:2	9126.0	00 ^h 15 ^m 26 ^s	+16°20'45"	0.54	2.25
SA 68	R11	00 15 41	+15 40 37	0.54	2.10
SA 68:2	6924.1	00 15 58	+16 09 33	0.54	2.07
SA 68:2	6924.0	00 15 58	+16 09 37	0.54	2.12
SA 68:2	7024.0	00 14 13	+16 14 59	0.785	1.90
SA 68:2	6947.0	00 14 13	+16 14 46	0.78	1.85
RW	3625	04 26 28	-36 52 16	0.34	1.81
RW	7860.1	04 26 31	-36 45 05	0.20	2.10
RW	11710.0	04 27 22	-36 39 20	0.18	2.03
RW	2296	04 27 23	-36 55 09	0.24	1.92
RW	6993	04 28 06	-36 46 06	0.04	1.93
RW	17615.1	04 28 30	-36 29 43	0.18	1.98
AB	1480.0	04 42 34	-18 45 23	0.51	1.71
AB	2417.0	04 42 20	-18 43 45	0.28	1.64
AB	13286.1	04 42 40	-18 24 29	0.10	2.16
Lynx	7116.0	08 41 07	+44 40 32	0.50	2.32
Lynx	2090.0	08 42 57	+44 51 23	0.205	2.00
Lynx	1932.0	08 42 59	+44 58 11	0.35	1.88
SA 57	2129.0	13 07 29	+29 23 44	0.41	2.13
SA 57	6884.2	13 04 57	+29 36 38	0.25	2.32
Hercules	7883	17 19 34	+50 03 49	0.29	2.24
Hercules	4320	17 19 43	+49 51 13	0.23	1.95
Hercules	7175	17 19 56	+50 01 36	0.32	2.17
Hercules	7494	17 18 18	+50 02 16	0.62	1.97
Hercules	7389	17 18 12	+50 01 55	0.62	2.02
Hercules	2672	17 18 05	+49 46 37	0.37	2.43

tion rate as an exponentially decaying function of time with an *e*-folding time τ . The initial mass function can be either the power-law form of Salpeter (1955) with any slope x to be specified, or the function can be that of the Miller and Scalo (1979) form.

To synthesize a spectrum, values of τ and x are chosen for a series of time intervals δt_i we calculate a galaxy spectrum for a time *t* to be

$$GS(t) = \sum_{\delta t} \sum_m \sum_k N_m(\delta t) p_m^k S_k,$$

where $N_m(\delta t)$ is the number of stars of mass *m* created in a time interval δt , *k* is the evolutionary state of the star, p_m^k is the probability that a star of mass *m* is in the *k*th stage, and S_k is the spectrum of the star in the *k*th stage and is treated like a vector, $S = S(\lambda)$. There is the additional constraint that

$$\sum_k p_m^k = 1,$$

where the sum is over all possible stages for a star of mass *m*. Two libraries of stellar spectrophotometry were used to synthesize a galaxy spectrum: those of Gunn and Stryker (1982) and Jacoby, Hunter, and Christian (1984). The Gunn-Stryker data range in wavelength from ~ 3100 Å to ~ 1.1 μ m but at a

TABLE 4
SPECTROPHOTOMETRIC SURVEY: SERENDIPITOUS GALAXIES

Field	Galaxy	α (1950.00)	δ (1950.00)	<i>z</i>	Break
SA 68:2	6808.0	00 ^h 15 ^m 57 ^s	+16°09'21"	0.54	1.44
SA 68:2	9126.5	00 15 25	+16 21 10	0.38	1.66
RW	426	04 28 32	-36 44 53	0.04	2.15
Hercules	2748.0	17 18 06	+49 46 25	0.29	1.66
Hercules	7175.5	0.32	2.00
Hercules	7389.5	0.61	1.62
SA 57	2129.5	0.42	1.55

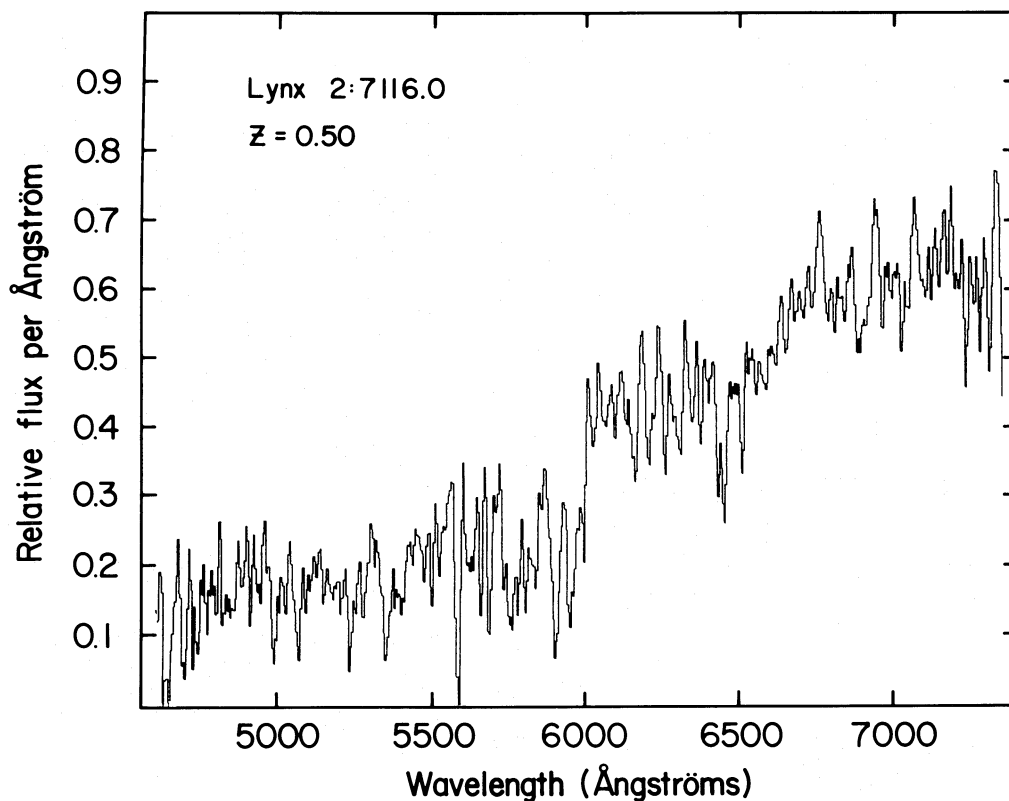


FIG. 11.—Observed spectrum obtained with cryogenic camera of program galaxy Lynx 2: 7116.0

coarse resolution of 10–20 Å per pixel. These data are excellent for synthesizing colors. When presented with a choice of stars of a given spectral type, we always chose the one with the stronger metallic lines; a metal-rich stellar library would have been more appropriate. The Hunter-Jacoby-Christian data range from about 3500 to 7500 Å and are at 1.54 Å per pixel, this sampling rate is good for measuring line indices such as those of $H\beta$ and Mg_2 .

The stellar evolutionary tracks compiled by Bruzual (1981) were used with only minor modifications. Because of the lack of detailed knowledge of how stars evolve past the first giant branch, these models are very crude: certain stellar species which must exist are not taken into account. Such is the case with the horizontal branch.

We decided not to include far-ultraviolet spectral energy distributions in the spectrum synthesis primarily because we do not observe rest frame flux densities below ~ 3500 Å. Also, there seems to be a large dispersion in the spectral energy distributions of nearby giant elliptical galaxies in the ultraviolet (Oke, Bertola, and Capaccioli 1981; Bertola, Capaccioli, and Oke 1982), and little is known about its origin.

We calculated, using both stellar libraries, evolutionary models of galaxy spectra for several epochs of observation ranging from 1 to 16 Gyr. We varied the e -folding time τ from 0.25 to 5 Gyr. We are only interested in those models which resemble giant elliptical galaxy spectra, and consequently we have limited our modeling appropriately. Based on the Gunn-Stryker catalog we calculated the 4000 Å break, ($u - g$), ($g - r$), ($r - i$), ($U - B$), ($B - V$), ($V - R$), and ($R - I$). The UBV response functions are from Johnson (1965), and RI are on the Kron-Cousins system (Bessell 1983). For the Hunter-Jacoby-Christian data, we calculated again the break, $H\beta$, Mg_2 , $Mg b$,

$TiO II$, NaD , and the G band. The information content of the $H\beta$ -index is contained within that of the break amplitude. The remaining line indices were found to contain little additional information. The definitions of these line indices are given in Faber *et al.* (1985).

The results of some of these computations are given in Figure 12. In this figure we give synthesized values of the color indices ($B - V$) and ($U - B$) and of the 4000 Å break amplitude as a function of age for several values of τ . The break amplitude or ($U - B$) are clearly more sensitive to an earlier turnoff than ($B - V$) or redder color indices. Additional diagrams similar to those of Figure 12 but for $ugri$ will be presented in Hamilton (1985); the photometric calibration is not yet finalized and the synthesized colors could be off as much as 0.15 mag. It is expected that in the limit of an old age the rate of change of all the colors of a single population of stars should decrease dramatically. Our results are consistent with that. Our modeling technique and the results of our models are similar to and consistent with those of Tinsley (1972a, c, 1980), Searle, Sargent, and Bagnuolo (1973), and Huchra (1977). The old age value of ($R - I$) is 0.88, and that of ($r - i$) is 1.10. These values are reached only a few Gyr after the onset of star formation and are independent of τ .

The behavior of the strength of $H\beta$ absorption with respect to time is similar to that of the 4000 Å break. The value of the $H\beta$ equivalent-width measurement for an age of 8 Gyr is 2.2 Å, and 1.6 Å for a galaxy twice that age. The observed $H\beta$ equivalent width for a giant elliptical galaxy is about 1.6 Å (Burstein *et al.* 1984).

Models were also generated with $x = 1.00$ and 2.00. The colors were basically the same, to within a few percent, as those for $x = 1.35$. Tinsley (1972c) and Searle, Sargent, and Bag-

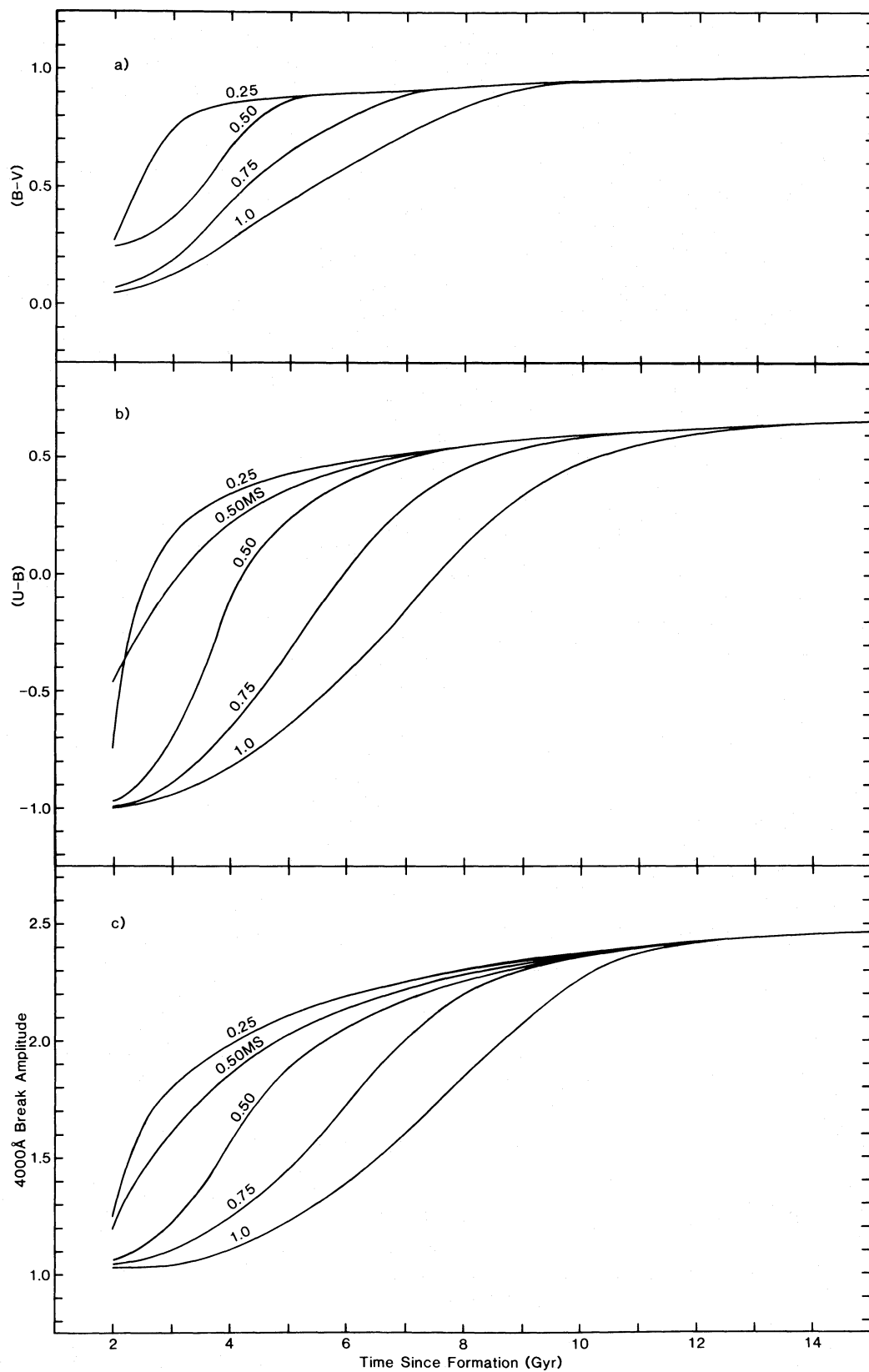


FIG. 12.—Predictions of the evolutionary models as discussed in § VI. (a) $(B-V)$ color index as a function of age, (b) $(U-B)$ color index as a function of age, (c) 4000 Å break amplitude as a function of age. The different curves are for various values of the star-formation e -folding time τ and for a Salpeter initial mass function with $x = 1.35$ (value for the solar neighborhood). The curves labeled 0.50MS are for $\tau = 0.50$ Gyr, and a Miller-Scalo initial mass function was used. In (a) the 0.50MS curve is identical with the 0.25 curve and has not been included.

nuolo (1973) also found that the colors were insensitive to x . This is to be expected, since the colors of the stars on the giant branch are, to first order, insensitive to the mass of the progenitor star. However, luminosity evolution is a sensitive function of x (Tinsley 1972c).

The zero-points for the $UBVRI$ synthesized colors are based on assuming that the colors of an averaged unreddened A0 V star are all identically zero. Typical errors in the colors, based on differences with real photometry, are approximately 0.05 mag.

In Figure 12 the curves labeled 0.50MS refer to $\tau = 0.50$ Gyr and a Miller-Scalo initial mass function. All the other curves were obtained by assuming a Salpeter initial mass function with $x = 1.35$. In Figure 12a, the 0.50MS curve is identical (within errors ± 0.05) to the $\tau = 0.25$ Gyr curve and therefore has not been included.

We have presented the colors and break amplitudes with respect to time and not redshift. In order to translate into the observable redshift, we need to assume values for the cosmological parameters H_0 and q_0 , as well as the time interval ($\Delta\tau_r$) between $t = 0$ and the first generation of stars. All models discussed below assume that ($\Delta\tau_r$) = 0.

VII. RESULTS AND DISCUSSION

a) The Evolution Diagram

The results of the spectrophotometric survey are presented in Figure 13. We have separated the program data (Fig. 13a) from the serendipitous data (Fig. 13b). There are several striking features of the redshift-break amplitude diagram (hereafter

called the evolution diagram). The most prominent feature of the program data is that there appears to be no systematic variation of the amplitude with respect to redshift, in contrast to that depicted in Figure 4 of Bruzual (1983) and in Spinrad (1980). (It is possible that the latter data could be explained entirely by color-gradient effects.) If, however, the two points at $z \approx 0.8$ in Figure 13a are actually defining the trend at high redshifts, then evolution may have been detected. Section VIIe is an interpretation from this point of view.

Linear least-squares fitting of the program data yield a y -intercept of 2.06 ± 0.09 (the mean of the data) and a slope of -0.07 ± 0.14 , which is consistent with zero. The correlation coefficient for the fit is -0.07 . We do not feel that it is fruitful to separate the UV SIT data from that of the cryogenic camera data because of the few data obtained with the UV SIT. The mean values of the break amplitudes for the two sets of data are the same. The dashed lines in Figure 13 are at a value of 2.06, the average of the program data. The average of Wells' spectrophotometry listed in Table 2 is 2.07 ± 0.10 .

If the serendipitous data are examined, the variation of amplitude with redshift is rather dramatic, although the statistics are rather few. Without further thought this could be claimed as evidence for evolution. It must be remembered, however, that as the sampling depth increases the typical galaxy becomes bluer in both $(g-r)$ and $(u-g)$. The latter color index is very similar to the break amplitude. The behavior of the serendipitous data in the evolution diagram can be explained entirely by the relation between color and absolute luminosity, i.e., as the sampling depth increases the characteristic absolute magnitude becomes fainter, hence bluer.

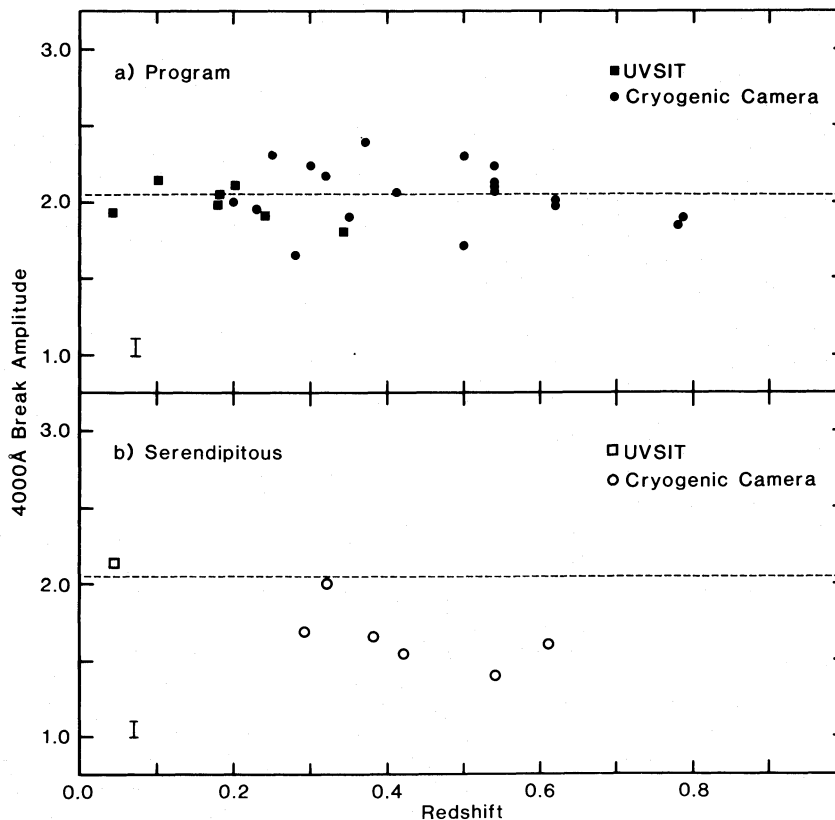


FIG. 13.—Evolution diagram or redshift-break amplitude relation for (a) the program galaxies and (b) the serendipitous galaxies. Error bars (lower left corner) indicate precision obtained with a single measurement of the break.

b) Predictions versus Observations

The old age model predictions of the UBV colors agree very well with the observed nuclear colors of NGC 4472, a giant elliptical galaxy in Virgo. The observed, dereddened color indices, $(B-V) = 0.95 \pm 0.03$ and $(U-B) = 0.60 \pm 0.05$, are from unpublished photometry by the author. We have adopted $E_{B-V} = 0.08$ for Virgo (O'Connell 1976).

The results of the computations of § VI indicate that the old age value of the break is ~ 2.4 . The observations, however, yield a value of 2.05. The difference could arise out of the neglect of certain stellar species, such as the asymptotic giant branch stars, in the modeling technique. The same effect would also show up in the UBV colors, yet the model predictions and colors of NGC 4472 agree rather well (to within 5%).

The discrepancy between observed and predicted break amplitudes is believed to be due to the applicability of the models to nuclear regions. This explanation is supported by the low- z measurements of the 4000 Å break in nearby elliptical galaxies by Spinrad as published in Bruzual (1983). Here the observed break values (for small apertures) are approximately 2.3. The remaining difference could easily be due to contamination from the outer portions of the galaxies.

This color-gradient effect would be less evident in the long-slit spectrophotometry, where the observed values are more nearly total or integrated. For one nonprogram galaxy we observed with the UV SIT, NGC 2217 (which is red by local standards), a 4000 Å break gradient was evident, declining from about 2.8 at the nucleus to about 2.1 at $10''$ from the nucleus. Certainly much more effort should be made to study gradients in late-type galaxies and to define either total quantities or quantities within a fixed metric aperture (here a "metric slit").

c) The Coevality of Galaxies

An assumption in this class of evolution models is that galaxies are coeval. The only recent argument on this point was by Sandage (1973), and his sample limit was at $z \approx 0.4$. He based his arguments on the narrowness of his $(B-V)$ data. Since the break amplitude is constant to within the errors to $z \approx 0.8$ for the program data, we can extend the validity of the assumption of approximate coevality to this redshift. In Figure 14, we show a histogram of the break amplitudes for the program data. Some of the width of this histogram is due to measurement error, but the predominant source of the spread is intrinsic, indicating a spread in ages (the departure of the observations from the assumption of true coevality). The intrinsic width indicates that the program galaxies are of the same age to within $\pm \sim 2$ Gyr. This is assuming that the value of τ is a universal constant obeyed by program galaxies. This is more certainly not the case, as distributions in both age and τ are more realistic. Variations in age or τ or both are inseparable.

Our measurements are probably not sensitive enough to distinguish between coevality and a sampling of progressively older galaxies with increasing look-back time. Before this can be explored further, the rest-frame color distributions and the absolute magnitude distributions will need to be derived. If we are sampling progressively older galaxies, then we should see a slight decrease in the average absolute magnitude with increasing look-back time.

d) The Ages of Galaxies

The evolutionary rate of change of the 4000 Å break can be described by the value of τ once the age of the system has been

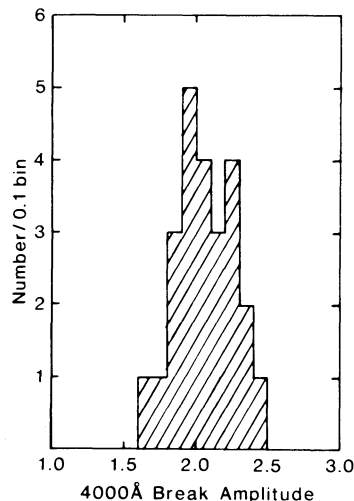


FIG. 14.—Distribution of values of break amplitude for all the program galaxies. Some of the width is due to measurement, but the majority is due to intrinsic variations.

specified. Fortunately, the determination of the ages of giant elliptical galaxies should be, in principle, independent of the value of H_0 , another yet unknown parameter. The currently accepted value for the age of giant elliptical galaxies is 16 Gyr and is based on the assumption that these systems must be as old as the oldest stars in the Galaxy. An alternative age, of about 8 Gyr, has been proposed by O'Connell (1980).

In order to specify the look-back time to a redshift of $z \approx 0.8$ we need to know both H_0 and q_0 , assuming Friedmann big bang cosmology with zero cosmological constant. The behavior of the look-back time at this redshift as a function of these two parameters is given in Figure 15. The contour lines are of equal look-back time and are given in Gyr. If we adopt $H_0 \approx 50 \text{ km s}^{-1} \text{ Mpc}^{-1}$, this implies that the look-back time at $z \approx 0.8$ is 7–8 Gyr, and this is only mildly dependent upon q_0 for any reasonable value. Clearly, if we adopt a present epoch age of 8 Gyr we should see a dramatic change in the value of the break at the high-redshift end, even if H_0 were as large as $100 \text{ km s}^{-1} \text{ Mpc}^{-1}$. Such behavior is not present in the data of the evolution diagram of Figure 13a. However, if we believe that the ages of galaxies are much larger, say 16 Gyr, then a $\tau \approx 0.9$ model adequately fits the observed data (see also § VIIe), where at $z \approx 0.8$ we are seeing galaxies at an age of 8–9 Gyr.

If it were possible for the present age of giant elliptical galaxies to be about 8 Gyr, then the value of H_0 has to be less than $70 \text{ km s}^{-1} \text{ Mpc}^{-1}$ for $q_0 \approx 0$ in order to account for the light travel time. If we accept an age of 16–17 Gyr, which, again, very adequately fits the observations, this leaves very little room for a strongly decelerated ($q_0 > 0.5$) universe if $H_0 \approx 50 \text{ km s}^{-1} \text{ Mpc}^{-1}$ and the cosmological constant is zero.

We have assumed in comparing models with observations that the last period of star formation is also the first. If all giant elliptical galaxies go through a period of significant star formation after initial creation, then we will have no sensitivity to the true ages of galaxies. We can only set lower limits. If, however, we allow the possibility that some galaxies could be described as a being formed from a single burst of star formation, then these would be redder than the multiple-burst versions, assuming that the time difference between the bursts is less than about 6 Gyr. Our selection criteria would then be choosing the single-burst objects over those with multiple bursts.

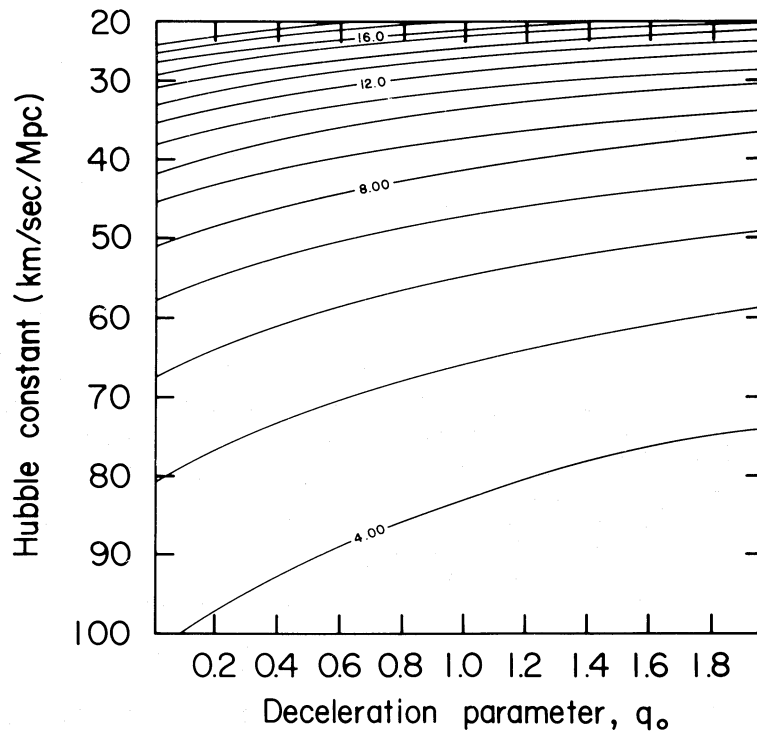


FIG. 15.—Contours are constant look-back time in Gyr for $z = 0.8$ as a function of H_0 and q_0 , for Friedmann cosmologies with zero cosmological constant

Both Bruzual (1983) and this paper (§ VI) demonstrate that the single-burst model adequately describes present-day giant elliptical galaxies.

e) Spectral Evolution versus Luminosity Evolution

The classical Hubble diagram is based on observations of first-ranked giant elliptical galaxies (Kristian, Sandage, and Westphal 1978; Gunn and Oke 1975). If effects of dynamical and spectral evolution are separable, then the evidence for no spectral evolution presented here of non-rich-cluster galaxies will also apply to their rich-cluster counterparts. We can give some observational support to this view because of the one rich-cluster galaxy that we did observe. The galaxy SA 68:2 6924 in our sample is one of the two brightest members of the core of the rich cluster of galaxies CL 0016+16. This object was chosen by our selection criteria for the spectrophotometric program. The value of the break amplitude for this object is 2.07, which is typical of the remainder of the program objects, which could be described as field galaxies.

For proper interpretation of the Hubble diagram, it is luminosity and not spectral evolution which is important. The critical parameter is the true shape of the luminosity function, and its parametrization as a power law is a misleading oversimplification.

Tinsley (1972c) has shown that, based on her models, luminosity evolution is greatest when the spectral (or color) evolution is least. Again, to make the additional step from color to luminosity evolution requires knowledge of the shape of the luminosity function, on which we are not willing to speculate. It is apparent, however, that the luminosity function is giant-dominated. This is an observational fact based on the Wing-Ford band measurements by Whitford (1977) and on the CO index measurements of Frogel *et al.* (1978) of nearby galaxies. A “dwarf-enriched” main sequence does not appear likely.

f) Interpretation of the Data for Evolution

Since the two program galaxies at $z \approx 0.8$ have break amplitudes slightly lower than the mean (but only 1–2 σ away), their lower values may not be due to noise but to evolutionary effects.

If we adopt $q_0 \approx 0$, $H_0 \approx 50 \text{ km s}^{-1} \text{ Mpc}^{-1}$, and $\tau = 0.9$ Gyr, we can then relate the observed relation (break amplitude vs. redshift) to that predicted by the evolutionary models (break amplitude vs. time). The difference we expect between break amplitudes for low z and $z \approx 0.8$ for $\tau \approx 0.90$ is only 7%. The observed difference is 7%. We cannot, therefore, separate the mild evolution case from that of no evolution. The results of the evolution diagram are consistent with both. Clearly, similar observations of galaxies in the redshift range $0.8 < z < 1.0$ are needed to verify the trends.

g) Comparisons with other Recent Investigations

A spectrophotometric survey by Oke (1984) of first-ranked cluster galaxies also indicates little change in the 4000 Å break to a redshift of $z \approx 0.8$. The selection criterion of Oke and collaborators was the morphological appearance of the cluster in one of four different single bandpass surveys conducted using different techniques. Oke’s sample comprises first-ranked galaxies in rich clusters of galaxies. We intentionally did not select these galaxies for our spectrophotometric program. It is encouraging that this investigation and that of Oke, which have distinctly different selection criteria, basically obtain the same result: no or very little spectral evolution to $z \approx 0.8$.

h) Further Observations

For the present survey it is unlikely that we could extend the evolution diagram, as currently defined, much beyond a redshift of $z \approx 1.0$. The signal-to-noise ratio of the photometry at

the faint-end ($r \approx 24$, $i \approx 22$) is becoming so small that we do not have the ability to select galaxies reliably based on ($r - i$) color. Additional problems also arise, in that at high redshifts the 4000 Å break is in the night sky OH forest where sky subtraction becomes difficult, the effect of telluric features is much greater in this region of the spectrum, and the sensitivity of most CCD chips is rapidly decreasing.

It may be more worthwhile to calibrate the 4000 Å break against some bluer spectral feature such as the 2900 Å break for a common set of data (if at all possible) and extend the evolution diagram to redshifts of about $z \approx 2$. Current technology will permit surveys of galaxies similar to those studied here to redshifts of $z \approx 1.5$. Advances in optical detector technology in the next decade are unlikely to be as dramatic as they were in the past one.

VIII. CONCLUSIONS

In a new deep spectrophotometric survey of giant elliptical galaxies we have found that the effects of an aging stellar population (spectral evolution) to a redshift of $z \approx 0.8$ change the 4000 Å break amplitude by less than 7% (look-back time of about 8 Gyr for $H_0 \approx 50 \text{ km s}^{-1} \text{ Mpc}^{-1}$ and $q_0 \sim 0$). This result is contrary to the more widely accepted belief that spectral evolution is a strong effect at even more nearby redshifts of $z \approx 0.5$. The evidence for a lack of strong spectral evolution presented here does not preclude, however, the possibility of strong luminosity evolution, knowledge of which is vital for the proper interpretation of the Hubble diagram.

We have demonstrated that the optical color selection of galaxies is a superior technique for selecting a more homogeneous sample of distant galaxies than other methods such as radio flux density, which is rather arbitrary, or selecting rich clusters of galaxies.

Our selection criterion was chosen to be redness in two-color diagrams. This selects galaxies which have had the least

star formation in the last ~ 6 Gyr and whose initial star formation was quite rapid.

The distribution of break amplitudes (assuming no evolution) indicates that the assumption of coevolution is valid only to within ± 2 Gyr. This distribution may be narrowed slightly by always choosing galaxies with exactly the same value of the rest frame color index.

The comparison of phenomenological models of spectral evolution with the observed data indicates that the present epoch age for giant elliptical galaxies is much older than 8 Gyr. These models adequately describe the evolution of giant elliptical galaxies with a present epoch age of about 16 Gyr and an exponentially decaying star-formation rate with an e -folding time of about 0.9 Gyr.

Within the context of the models of spectral evolution, the data are consistent with $H_0 \approx 50 \text{ km s}^{-1} \text{ Mpc}^{-1}$ and $q_0 \approx 0$. The data are inconsistent with $H_0 \gtrsim 70 \text{ km s}^{-1} \text{ Mpc}^{-1}$. A strongly decelerated universe ($q_0 > 0.5$) is possible only if $H_0 \lesssim 32 \text{ km s}^{-1} \text{ Mpc}^{-1}$.

Observations of galaxies selected in a similar manner as our program galaxies will provide valuable information on the star-formation history of these giant elliptical galaxies.

I am grateful for the support provided by Geoffrey Burbidge, Hyron Spinrad, Richard Kron, and Roger Hildebrand over the course of this work. Frank Valdes, Doug Tody, Jeannette Barnes, and Roger Lynds tolerated the many hours of reduction and computation at Kitt Peak. I wish to thank Oscar Saa, Daniel Maturana, Riccardo Venegas, and especially George Will for assistance at the telescopes. Sollie Lucero, the late Don Powers, Earl O'Neil, and Richard Dreiser also contributed to the success of this work. Funding was provided in part by private sources and by a consultantship with Bell Laboratories in 1983–1984.

REFERENCES

- Baum, W. A. 1959, *Pub. A.S.P.*, **71**, 106.
 Bertola, F., Capaccioli, M., and Oke, J. B. 1982, *Ap. J.*, **254**, 494.
 Bessel, M. 1983, *Pub. A.S.P.*, **95**, 480.
 Brown, G. S., and Tinsley, B. M. 1975, *Ap. J.*, **194**, 555.
 Bruzual, A. G. 1981, Ph.D. thesis, University of California, Berkeley.
 ———. 1983, *Ap. J.*, **273**, 105.
 Burstein, D., Faber, S., Gaskell, C., and Krumm, N. 1984, *Ap. J.*, **287**, 586.
 Burstein, D., and Heiles, C. 1982, *A.J.*, **87**, 1165.
 Djorgovski, G., Spinrad, H., and Marr, J. 1984, preprint.
 Faber, S. 1972, *Astr. Ap.*, **20**, 361.
 ———. 1973, *Ap. J.*, **179**, 731.
 ———. 1977, in *The Evolution of Galaxies and Stellar Populations*, ed. B. M. Tinsley and R. B. Larson (New Haven: Yale University Press), p. 157.
 Faber, S., Friel, E., Burstein, D., and Gaskell, C. 1985, *Ap. J. Suppl.*, **57**, 711.
 Fitch, W., and Morgan, W. W. 1951, *Ap. J.*, **114**, 548.
 Frogel, J. A., Persson, S. E., Aaronson, M., and Matthews, K. 1978, *Ap. J.*, **220**, 75.
 Gunn, J. E., and Oke, J. B. 1975, *Ap. J.*, **195**, 255.
 Gunn, J. E., and Stryker, L. L. 1982, *Ap. J. Suppl.*, **52**, 121.
 Hamilton, D. 1983, in *IAU Colloquium 78, Astronomy with Schmidt-type Telescopes*, ed. M. Capaccioli (Dordrecht: Reidel), p. 461.
 ———. 1985, in preparation.
 Hayes, D. S., and Latham, D. W. 1975, *Ap. J.*, **197**, 593.
 Heckman, T., Balick, B., and Crane, P. 1980, *Astr. Ap. Suppl.*, **40**, 295.
 Hubble, E., and Tolman, R. C. 1935, *Ap. J.*, **82**, 302.
 Huchra, J. 1977, *Ap. J.*, **217**, 928.
 Iben, I. 1967, *Ann. Rev. Astr. Ap.*, **5**, 571.
 Jacoby, G. H., Hunter, D. A., and Christian, C. A. 1984, *Ap. J. Suppl.*, **56**, 257.
 Johnson, H. L. 1965, *Ap. J.*, **141**, 923.
 Kristian, J., Sandage, A., and Westphal, J. 1978, *Ap. J.*, **221**, 383.
 Kron, R. G. 1978, Ph.D. thesis, University of California, Berkeley.
 ———. 1980, *Phys. Scripta*, **21**, 652.
 Longo, G., and de Vaucouleurs, A. 1983, Univ. of Texas Pub.
 Miller, G. E., and Scalo, J. M. 1979, *Ap. J. Suppl.*, **41**, 513.
 Miller, J. S., and Mathews, W. G. 1972, *Ap. J.*, **172**, 593.
 Mould, J. R. 1978, *Ap. J.*, **220**, 434.
 O'Connell, R. W. 1973, *A.J.*, **78**, 1074.
 ———. 1976, *Ap. J.*, **206**, 370.
 ———. 1980, *Ap. J.*, **236**, 430.
 Öhman, Y. 1934, *Ap. J.*, **80**, 71.
 Oke, J. B. 1971, *Ap. J.*, **170**, 193.
 ———. 1974, *Ap. J. Suppl.*, **27**, 21.
 ———. 1984, in *Clusters and Groups of Galaxies*, ed. F. Mardirossian, G. Giuricin, and M. Mezzetti (Dordrecht: Reidel), p. 99.
 Oke, J. B., Bertola, F., and Capaccioli, M. 1981, *Ap. J.*, **243**, 453.
 Oke, J. B., and Gunn, J. E. 1983, *Ap. J.*, **266**, 713.
 Renzini, A. 1981, *Ann. Phys. (Paris)*, **6**, 87.
 Renzini, A., and Buzzoni, A. 1983, *Mem. Soc. Astr. Italiana*, **54**, 739.
 Salpeter, E. 1955, *Ap. J.*, **121**, 161.
 Sandage, A. 1972a, *Ap. J.*, **176**, 21.
 ———. 1972b, *Ap. J.*, **178**, 25.
 ———. 1973, *Ap. J.*, **183**, 711.
 Schoening, W. E. 1978, *AAS Photo-Bull.*, **17**, 12.
 Searle, L., Sargent, W. L. W., and Bagnuolo, W. 1973, *Ap. J.*, **179**, 427.
 Spinrad, H. 1961, *Ap. J.*, **135**, 715.
 ———. 1977, in *The Evolution of Galaxies and Stellar Populations*, ed. B. M. Tinsley and R. B. Larson (New Haven: Yale University Press), p. 301.
 ———. 1980, in *IAU Symposium 104, Objects of High Redshift*, ed. G. O. Abell and P. J. E. Peebles (Dordrecht: Reidel), p. 39.
 Spinrad, H., and Taylor, B. J. 1971, *Ap. J. Suppl.*, **22**, 445.
 Stone, R. P. S., and Baldwin, J. 1983, *M.N.R.A.S.*, **204**, 347.
 Strömgen, B. 1966, *Ann. Rev. Astr. Ap.*, **4**, 433.
 Tift, W. G. 1969, *A.J.*, **74**, 354.
 Tinsley, B. 1967, Ph.D. thesis, University of Texas, Austin.
 ———. 1972a, *Astr. Ap.*, **20**, 383.
 ———. 1972b, *Ap. J. (Letters)*, **173**, L93.
 ———. 1972c, *Ap. J.*, **178**, 319.
 ———. 1977, *Ap. J.*, **211**, 621.

- Tinsley, B. 1980, *Ap. J.*, **241**, 41.
Tinsley, B., and Gunn, J. E. 1976, *Ap. J.*, **203**, 52.
Valdes, F. 1983a, *FOCAS, Faint Object Classification and Analysis System* (KPNO User's Manual).
———. 1983b, *SPIE*, **331**, 465.
van den Bergh, S. 1963, *A.J.*, **68**, 413.
———. 1975, *Ann. Rev. Astr. Ap.*, **13**, 217.
van den Bergh, S., and Sackmann, I. J. 1965, *A.J.*, **70**, 353.
Visvanathan, N., and Sandage, A. 1977, *Ap. J.*, **216**, 214.
Wells, D. 1972, Ph.D. thesis, University of Texas.
Whitford, A. E. 1958, *A.J.*, **63**, 201.
———. 1971, *Ap. J.*, **169**, 215.
———. 1977, *Ap. J.*, **211**, 527.
Wilkinson, A., and Oke, J. B. 1978, *Ap. J.*, **220**, 376.
Zinn, R. 1980, *Ap. J. Suppl.*, **42**, 19.

DONALD HAMILTON: National Optical Astronomy Observatories, P.O. Box 26732, 950 North Cherry Avenue, Tucson, AZ 85726-6732